ce/papers Proceedings in civil engineering
eurosteel CRACOW 2026
WILEY

Full paper

Numerical and Neural Network Investigation of a New Dual Self-centering Energy Dissipation Device

Vasileios C. Kamperidis[1] | Dan V. Bompa[2] | Georgios Chliveros[3] | Themelina S. Paraskeva[4] | Konstantinos N. Kalfas[5] | John Bellos[1]

Correspondence

Dr. Vasileios C. Kamperidis
Neapolis University Pafos, Department of Civil Engineering, Paphos, CY, 8042, Cyprus
Email: v.kamperidis@nup.ac.cy

[1] Neapolis University Pafos, Paphos, Cyprus
[2] University of Surrey, Guildford, United Kingdom
[3] Metropolitan College, Marousi Campus, Greece
[4] Edith Cowan University, Joondalup, Perth, WA 6027, Australia
[5] Texas State University, Ingram School of Engineering, Texas, 78666, USA

Abstract

Proposed self-centering (SC) seismic systems can reduce residual drift, but their SC and energy-dissipating (ED) solutions often face limitations, including reliance on yielding components, full-bay tendon layouts, and detailing complexity in beam-column connections. This paper investigates a compact SC-ED sub-assembly comprising a high-strength post-tensioned multi-wire steel tendon routed in a 180° path around a roller bearing, with both tendon ends aligned. A three-dimensional nonlinear finite element (FE) workflow, building on earlier numerical work and selectively refined here, is used to evaluate response under a displacement-controlled cyclic protocol representative of seismic demands. Results show stable flag-shaped hysteresis without residual displacement and elastic behaviour of the primary components. ED is interpreted as arising from tendon-bearing interface friction and curvature-activated internal mechanisms in the multi-wire tendon. An artificial neural network (ANN) surrogate model trained on force-displacement data reproduces the nonlinear response on unseen data, enabling rapid prediction. The study demonstrates the feasibility of a tribology-driven curved tendon-bearing SC-ED sub-assembly for seismic-resilient structural connections.

Keywords

Self-centering, Energy Dissipation, Seismic Design, Artificial Neural Network (ANN), Structural Connection, Seismic Resilience

1 Introduction

1.1 Background and motivation

Self-centering (SC) seismic technologies reduce residual drifts while providing supplemental energy dissipation (ED) under cyclic loading [1]. A key challenge is achieving stable hysteretic dissipation without compromising the restoring force for self-centering [2–3]. Integrating SC–ED devices into seismic-resisting systems can reduce damage, interstorey drifts and collapse risk under far- and near-fault earthquakes [4–5]. More broadly, recent state-of-the-art reviews show that the motivation for SC and SC-ED systems lies in overcoming the residual deformation, repairability and functional-recovery limitations of conventional seismic-resistant systems, especially in steel structures and their beam–column connections [6–7].

For beam–column connections, existing SC-ED solutions may be grouped broadly into post-tensioned (PT) steel connections with yielding or friction-based ED devices, PT precast concrete hybrid connections, and shape-memory-alloy (SMA)-based SC connections [6–7]. Despite significant progress, these families retain well-documented limitations that have constrained wider uptake in practice: lower intrinsic hysteretic ED than conventional ductile systems, dependence on yielding fuses with associated inspection, fatigue and replaceability concerns, and implementation and constructability difficulties, including layouts that cannot always be used in both joint directions and tendon arrangements that run over the full bay length and may interfere with services [6–7]. Thus, what remains unresolved in such connections is a compact SC-ED sub-assembly that dissipates energy through non-yielding mechanisms, remains local to the joint region, avoids full-bay tendon runs, and keeps primary components elastic during seismic response [6–7].

In this context, this paper investigates a compact dual SC–ED sub-assembly/device (DSCEDD) comprising (i) a high-strength multi-wire steel tendon that provides restoring

https://doi.org/10.1002/cepa.70795

force and participates in ED; and (ii) a roller bearing that redirects the tendon. The FE workflow builds on the earlier numerical study of Oryem [8] and is revisited here with targeted modelling refinements, a mechanism-based interpretation, and an Artificial Neural Network (ANN) surrogate model. The novelty lies in placing the DSCEDD in a realistic seismic-resilient SC connection context and bridging two usually separate perspectives: (i) seismic SC-ED devices, typically assessed through global hysteresis and reduced-order tendon idealisations; and (ii) routed tendon/rope mechanics over deviation elements, where wrap effects, contact traction, and curvature-induced micro-slip govern ED and stress localisation. Here, a multi-wire tendon is routed through a 180° bearing deviation path and analysed under a seismic protocol using 3D contact/friction FE modelling, so that deviation-zone mechanics and stress localisation are captured explicitly and interpreted through the ED taxonomy of Table 1 [9–11].

1.2 ED in tendon–pulley/tendon–bearing systems

ED in tendon–bearing/tendon–pulley systems can arise from concurrent mechanisms: (M1) interface traction and sliding friction at the tendon–bearing contact; (M2) interwire friction within the multi-wire tendon under cyclic axial loading; (M3) curvature-induced self-damping under combined tension–bending states; and (M4) longer-term degradation processes (wear/fretting evolution) that may alter ED capacity. These mechanisms are supported by cable–pulley ED systems [9, 12], traction/contact modelling in rope–sheave systems [10], and multi-wire tendon/strand mechanics under tension–bending and internal friction [13–19].

Curvature is central because wrap can produce tension redistribution and traction amplification, consistent with Euler–Eytelwein (capstan/belt-friction) behaviour [11]. In SC systems with multi-wire tendons, hysteretic response may reflect the combined action of these mechanisms, helping explain why simplified numerical models can predict narrower loops than experimental ones; μ should therefore be treated as an effective modelling parameter and checked via sensitivity where feasible when frictional ED is a primary driver [20–23].

Table 1 Mechanism map (taxonomy) for potential ED sources in the investigated sub-assembly

ID	Mechanism	How it is activated in this device	Key supporting literature
M1	Interface friction at tendon–bearing contact (macro-slip / micro-slip)	Imposed cyclic displacement activates sliding/traction at the tendon-bearing contact.	Han et al. [10]; Hernandez et al. [12]; Qin et al. [9]
M2	Interwire friction under axial cycling (wire-to-wire stick-slip)	Multi-wire tendon develops contact pressure among wires; cyclic tension promotes microslip and frictional loss.	Poon et al. [24]; Hong et al. [13]; Montoya et al. [25]
M3	Curvature-induced self-damping under bending (interwire microslip driven by cyclic curvature)	Tendon is wrapped/redirected over the bearing causing curvature; cyclic motion produces repeated bending and local relative slip.	Foti & Martinelli [18]; Foti et al. [17]; Chen et al. [14]; Papailiou [15]; Yu et al. [19]
M4	Inelasticity / fretting / wear-related dissipation and degradation (secondary, long-term)	If local stresses exceed elastic range or fretting evolves at contacts, plastic work and wear can contribute and degrade response.	Fontanari et al. [26]; Ivanov et al. [27]; Chang et al. [28]

1.3 Scope and contributions

This paper addresses: (a) concept development and intended performance of the DSCEDD; (b) standalone numerical and ANN investigation under a seismic protocol; and (c) qualitative identification of ED mechanisms without quantifying their energy shares. The DSCEDD design is embedded in a connection context for realism, but connection-level detailing, fatigue damage, and wear evolution are out of scope. Key contributions are: (i) the ED taxonomy of Table 1; (ii) a 3D nonlinear FE workflow with explicit contact/friction for a curved multi-wire tendon over a roller bearing; (iii) stable cyclic hysteresis with SC relative to the prestressed reference state; (iv) tendon stress-demand verification (917 MPa ≈56% of yield); and (v) ANN surrogate learning of the FE force-displacement response for rapid prediction.

2 Description of the DSCEDD Sub-assembly

The DSCEDD is a compact standalone SC–ED sub-assembly comprising (i) a roller bearing that redirects the tendon and (ii) a high-strength multi-wire steel tendon that provides restoring force and contributes to dissipation. Figure 1(a) shows the sub-assembly: routing, loading, boundary conditions (BCs), and ED mechanisms; Figure 1(b) shows a representative connection-level application context (connection details are out of scope). The investigated configuration considered herein is a toroidal roller bearing with a three-strand multi-wire tendon routed along a 180° curved path around the bearing external surface. Auxiliary components (cap rings/central rod) enforce the tendon path and anchorage. Specification and modelling parameters are summarised in Tables 2–3.

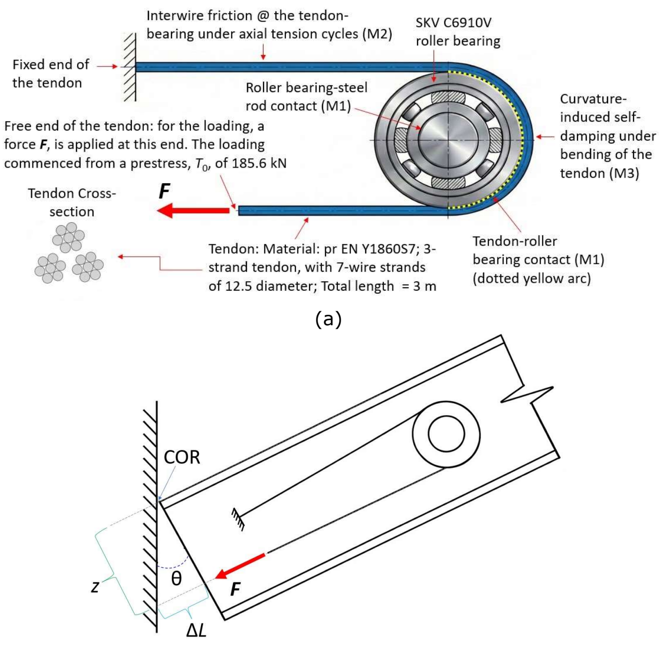

Figure 1 (a) Schematic of the DSCEDD with its loading, BCs, tribological conditions and ED mechanisms; and (b) Function and deformed geometry of the DSCEDD in a hypothetical structural connection.

Table 2 Investigated DSCEDD configuration

Item	Adopted specification used in this paper	Notes / source
Bearing type	CARB toroidal roller bearing	SKF C 6910 V [29]
Bearing main dimensions	d = 50 mm (bore), D = 72 mm (OD), B = 40 mm (width)	SKF C 6910 V [29]
Tendon type	Multi-wire tendon comprising 3 strands	Adopted PT configuration
Strand layup	1×7 per strand	Adopted strand configuration
Nominal strand diameter	12.5 mm	VSL International Ltd [30]
Wire diameter	4.12 mm	Geometric derivation from 12.5 mm 1×7 strand
Tendon total area	279 mm²	VSL International Ltd [30]
Tendon routing	180° curved path around bearing external surface; tendon ends aligned	Adopted device geometry
Tendon geometric construction	Circular tendon profile swept/extruded along curved trajectory around the bearing	SOLIDWORKS sweep/extrude implementation
Imposed tendon twist	5 revolutions along tendon length	Du et al. [31]
Auxiliary components	Cap rings and central rod (guiding/anchorage)	Ensures intended tendon path and BCs.
Central rod modelling note	Rod diameter taken slightly smaller than bearing bore (e.g., ≈49.5 mm)	Avoids over-closure / assembly interference.

Table 3 Adopted modelling parameters and loading

Category	Parameter	Adopted value used	Notes / source
Prestress	Tendon prestress force (T_0)	185.2 kN	Adopted FE value
Prestress	Reference tendon elongation	~10 mm	Treated as “re-centered” reference state
Material	Steel elastic modulus (E)	≈200 GPa	Nominal steel property
Material	Poisson’s ratio (ν)	≈0.30	Nominal steel property
Contact	Tangential behaviour	Coulomb friction	-
Contact	Friction coefficient	μ = 0.2	Representative contact value [16, 19, 22]
Seismic protocol	Reference standard	AISC 341-16	[32]
Seismic protocol	Drift demand	up to 0.04 rad	AISC 341-16 [32]
Seismic protocol	Equivalent peak displacement	9.6 mm	Derived from geometry and target drift
Analysis sequence	Stage 1	Prestress / pretensioning	-
Analysis sequence	Stage 2	Cyclic displacement-controlled loading	-

3 Nonlinear FEM modelling and analysis

A 3D nonlinear FEM workflow, building on the earlier numerical study of Oryem [8], was selectively refined to evaluate the cyclic response of the tendon–bearing DSCEDD. The assembly geometry was created in SOLIDWORKS [33], preliminary checks were conducted in Abaqus/CAE and Abaqus/Standard [34], and the final nonlinear contact simulations were performed in ANSYS Mechanical [35].

Figure 2 summarises the DSCEDD FE assembly and key components included in the model (bearing, routed tendon and auxiliary guiding/anchorage parts) to reproduce the intended load path. The routed tendon geometry is generated by sweeping/extruding a circular profile along the prescribed curved trajectory around the bearing external surface (180° deviation). Mesh refinement is concentrated in the deviation zone where stress gradients and contact traction are expected to localise.

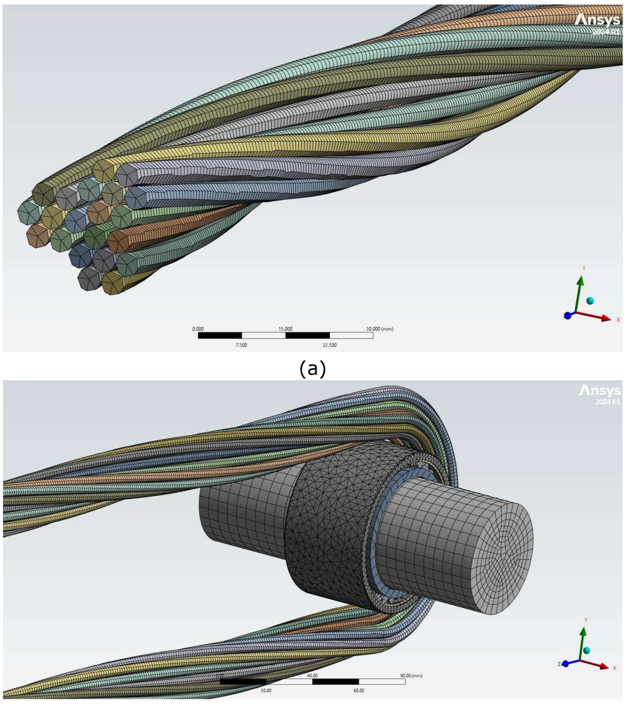

Figure 2 Meshing of the tendon (a) and of the bearing/rod (b)

Figure 3 illustrates the contact/friction interfaces and the BCs used to enforce tendon-end alignment and the intended tendon routing around the bearing. Surface-to-surface finite-sliding contact is defined at the tendon–bearing interface, with Coulomb friction. A value μ≈0.2 is adopted as an effective steel/strand contact parameter, consistent with representative strand/contact studies [16, 19, 22]. Primary components are modelled with linear-elastic steel response in the investigated configuration. While the present solid-tendon idealisation does not resolve individual wires explicitly, additional dissipation contributions associated with internal strand mechanics under combined tension–curvature (M2–M3) are discussed mechanistically in light of multi-wire tendon/strand literature [13–19].

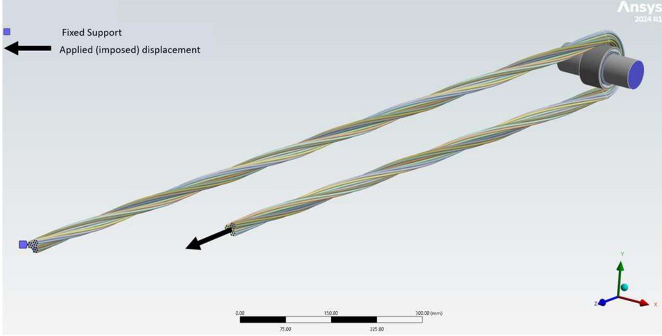

Figure 3 BCs in the FEM model

Figure 4 presents the loading sequence adopted in the FE analysis. The analysis is executed in two sequential steps: (i) prestress is applied to establish a stable reference configuration; for the adopted FE case, the prestress force is 185.2 kN (≈10 mm tendon extension), which defines the reference state for cyclic response evaluation; and (ii) displacement-controlled cycling is imposed (at the lower tendon end, as per Figure 3) following the AISC protocol [32]. The adopted peak displacement (≈9.6 mm) corresponds to a deformation level of approximately 0.04 rad when mapped through the assumed lever arm; this level is commonly used for special moment-frame (SMF) connection qualification in AISC contexts [32] and is comparable to EC8 plastic hinge rotation-capacity benchmarks for dissipative connections (e.g., 35 mrad for DCH) [36].

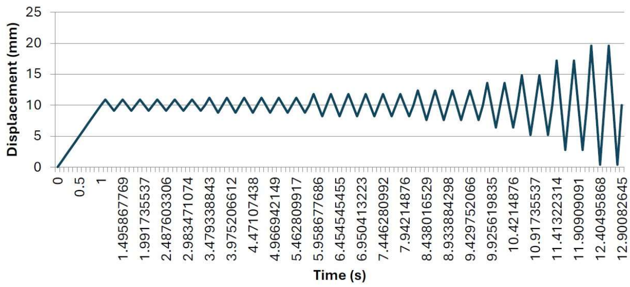

Figure 4 Loading sequence as applied in the FEM model: Imposed displacement at the tendon free end, versus time

4 Results: hysteresis and energy dissipation

Figure 5 presents the force–displacement hysteresis obtained from the nonlinear FE analysis. The response is stable and repeatable under the imposed protocol, with broadly symmetric loops and peak reaction forces on the order of ±400 kN over an approximately ±10 mm displacement range. Self-centering is interpreted relative to the prestressed reference configuration, i.e., the response returns close to the prestressed state after each cycle rather than to the zero-prestress state. The hysteresis area in Figure 5 indicates appreciable dissipation while maintaining restoring behaviour. In the present modelling framework, dissipation is primarily attributed to tendon–bearing frictional contact at the deviation zone (M1), while additional mechanisms linked to multi-wire tendon behaviour under cyclic tension and sustained curvature (M2–M3) provide a rational interpretation without requiring yielding of primary components [13–19].

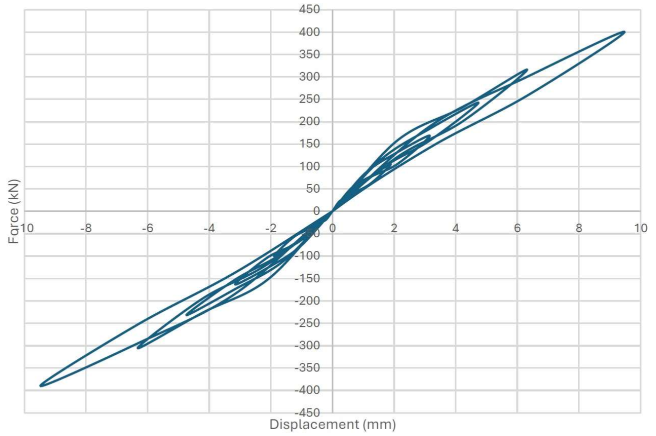

Figure 5 Force–displacement hysteresis from the FEM analysis

Figure 6 shows the stress distribution in the sub-assembly at maximum imposed displacement. Peak tendon stress is 917 MPa (≈56% of the tendon yield strength, 1634 MPa), confirming elastic response in the investigated configuration. The stress contours localise demands at the deviation zone, consistent with curvature-activated contact/traction effects. A value $\mu \approx 0.2$ is adopted here as an effective steel/strand contact parameter, consistent with representative strand/contact studies [16, 19, 22]; because μ depends on pressure/surface state and may evolve with cycling, sensitivity checks are recommended where feasible when frictional ED is a primary driver [20–23].

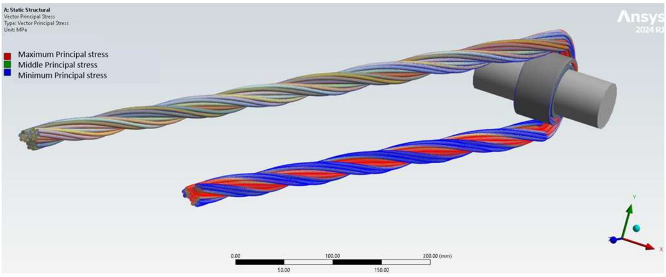

Figure 6 Principal-stress distribution at maximum imposed displacement in the tendon–bearing sub-assembly

5 Results and ANN-based surrogate modelling

The nonlinear FE response under displacement-controlled cycling yields stable hysteresis with near-perfect self-centering relative to the prestressed reference state (Figure 5), while primary components remain elastic in the investigated configuration (peak tendon stress 917 MPa). A key insight is that appreciable ED is achieved in a high-stress yet elastic tendon regime under sustained curvature, where deviation-zone contact/traction is activated during reversed cycling and reflected in both hysteresis area (Figure 5) and stress localisation (Figure 6). To enable rapid prediction of the nonlinear cyclic response for parametric studies, an ANN surrogate was trained using the FEM-generated force–displacement dataset. The ANN model can be used as a rapid predictor of new unseen data points for similar structures, avoiding the need to re-run a new FE simulation. In this sense, it acts as a surrogate to the FEM model, since it is trained on data generated by the FEM analyses.

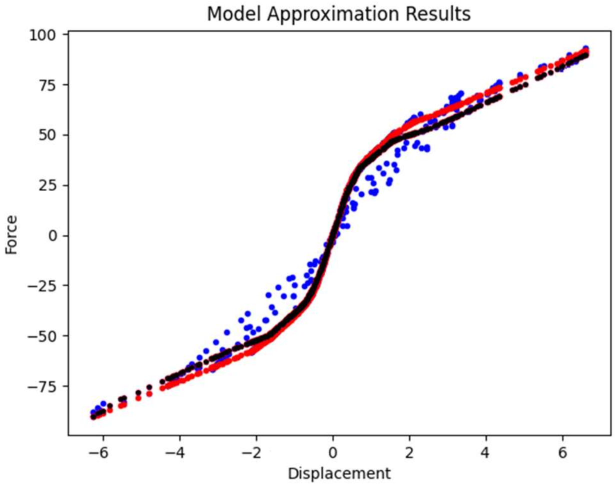

Figure 7 Force–displacement response predicted by the MLP model, showing the MAE-based prediction (red), the MSE-based prediction (black), and the testing data points (blue).

A feedforward NN, namely a multilayer perceptron (MLP), was employed and trained using adaptive moment estimation with Mean Squared Error (MSE) and Mean Absolute Error (MAE) loss functions. The Rectified Linear Unit (ReLU) was adopted as the activation function. Its derivative was used during backpropagation to update the weights and biases so as to minimise either the MAE or the MSE loss. In general, MAE is less sensitive to outliers and, for the present load curve, was expected to provide a closer representation of the target response than MSE. Training was performed using exclusively simulated (FE) data, with a 60:40 train–test split over the full dataset. The trained model was then tested on a random 40% subset of the dataset within the displacement range (-6, 6), in order to avoid overfitting in the outer simulation regions (-8, -6) and (6, 8), and in the scattered data [37–40]. As shown in Figure 7, the practical significance of the MAE- versus MSE-based training is that the MAE model better follows the physics-informed shape expected for the force–displacement response: concave upward for positive displacement and concave downward for negative displacement. The MAE-based model therefore reproduces the theoretically expected behaviour more closely than the MSE-based model.

6 Discussion

The FE and ANN results support DSCEDD feasibility and potential integration into seismic-resilient SC structural connections: FE analysis indicates repeatable dissipation and SC while keeping primary components elastic, and the ANN surrogate reproduces the force-displacement response, with MAE matching the response better than MSE. Key sensitivities remain associated with BCs, interface assumptions, lack of mechanism-wise ED decomposition, and ANN training only on FE-generated data.

Although hysteresis is stable in the analysed cycles, the simulations use elastic material behaviour with Coulomb friction and do not include fatigue-damage or wear-evolution modelling; long-term durability therefore requires dedicated fatigue/wear analyses and/or experiments, particularly because curved tendon routing imposes cyclic bending strain regimes in wire ropes/strands [41] and is central to bending-over-sheave fatigue-life assessment for rotation-resistant ropes [42].

7 Conclusions and future research

This work investigates a compact DSCEDD comprising a routed multi-wire steel tendon and a roller bearing, intended for use in structural joints. The tendon provides restoring force for SC, while the bearing redirects the tendon and activates friction- and curvature-driven ED at the deviation zone, keeping the joint local. A 3D contact/friction FEM workflow is used under a seismic protocol, and an ANN surrogate is trained to emulate the FEM force–displacement response. Main conclusions are:

1. The DSCEDD exhibits stable, broadly symmetric hysteresis with near-perfect SC relative to the prestressed reference state, indicating repeatable ED without primary-component yielding.
2. The results highlight an underexplored regime for seismic devices: a multi-wire tendon under high elastic stress and sustained curvature (180° routing) dissipates energy through deviation-zone traction and curvature-driven internal mechanisms under fully reversed cyclic loading.
3. Peak tendon stress is 917 MPa (≈56% of yield), and stress contours localise demands at the deviation zone at maximum displacement, supporting the mechanics-based ED interpretation of Table 1.
4. The ANN surrogate reproduces the FE force–displacement response and enables rapid prediction for screening and optimisation.

Future work should (i) quantify energy shares from competing mechanisms (M1–M3) via targeted post-processing and/or higher-fidelity models, (ii) evaluate sensitivity to μ and interface state evolution, and (iii) assess long-term durability through fatigue/wear modelling and experimental validation for bending-over-deviation scenarios.

References

[1] Kamperidis, V. C. (2016) Novel Damage-Free Self-Centering Column Base Connection for Earthquake-Resilient Steel Buildings. PhD Dissertation, University of Warwick.

[2] Kamperidis, V. C.; Karavasilis, T. L.; Vasdravellis, G. (2015) Design and modeling of a novel damage-free steel column base. In: The Eighth International Conference on Advances in Steel Structures (ICASS 2015), Lisbon, Portugal, July 22–24, Paper No. 118.

[3] Kamperidis, V. C.; Karavasilis, T. L.; Vasdravellis, G. (2018) Self-centering steel column base with metallic energy dissipation devices. J. Constr. Steel Res. 149.

[4] Kamperidis, V. C.; Papavasileiou, G. S.; Kamaris, G. S.; Vasdravellis, G. (2020) Seismic collapse of self-centering steel MRFs with different column base structural properties. J. Constr. Steel Res. 175, 106364.

[5] Kamaris, G. S.; Papavasileiou, G. S.; Kamperidis, V. C.; Vasdravellis, G. (2022) Residual drift risk of self-centering steel MRFs with novel steel column bases in near-fault regions. Soil Dyn. Earthq. Eng. 162, 107391.

[6] Fang, C.; Wang, W.; Qiu, C.; Hu, S.; MacRae, G. A.; Eatherton, M. R. (2022) Seismic resilient steel structures: A review of research, practice, challenges and opportunities. J. Constr. Steel Res. 191, 107172.

[7] Zhong, C.; Christopoulos, C. (2022) Self-centering seismic-resistant structures: Historical overview and state-

of-the-art. Earthq. Spectra 38, pp. 1321–1356.

[8] Oryem, H. (2024) Numerical Investigation of Energy Dissipation of a New Seismic Self-Centering Device [Master's dissertation]. University of Surrey, UK.

[9] Qin, H.; Milani, G.; Bi, K.; Dong, H.; Du, X. (2025) A novel cable-pulley based self-centering energy dissipation (CP-SCED) brace for seismic induced damage mitigation of RC double-column bridge piers. Eng. Struct. 333, 120130.

[10] Han, Y.; Hu, H.; Sun, H.; Shi, X. (2025) A new rope-sheave traction contact force model incorporating complex geometric features developed through parameter identification methods. Appl. Math. Mech. 46, pp. 1983–2006.

[11] Lubarda, V. A. (2014) The mechanics of belt friction revisited. Int. J. Mech. Eng. Educ. 42, pp. 97–112.

[12] Hernández, F.; Astroza, R.; Beltrán, J. F.; Zhang, X.; Mercado, V. (2022) An experimental study of a cable-pulleys spring-damper energy dissipation system for buildings. J. Build. Eng. 51, 104034.

[13] Hong, K.-J.; Yi, C.; Lee, Y. (2012) Geometry and friction of helically wrapped wires in a cable subjected to tension and bending. Int. J. Steel Struct. 12, pp. 233–242.

[14] Chen, Y.; Meng, F.; Gong, X. (2017) Study on performance of bended spiral strand with interwire frictional contact. Int. J. Mech. Sci. 128–129, pp. 499–511.

[15] Papailiou, K. O. (1995) Bending of Helically Twisted Cables under Variable Bending Stiffness Due to Internal Friction, Tensile Force and Cable Curvature. Doctor of Technical Sciences thesis, ETH Zurich, Switzerland.

[16] Foti, F.; Martinelli, L. (2016) Mechanical modeling of metallic strands subjected to tension, torsion and bending. Int. J. Solids Struct. 91, pp. 1–17.

[17] Foti, F.; Martinelli, L.; Perotti, F. (2017) A parametric study on the structural damping of suspended cables. Procedia Eng. 199, pp. 140–145.

[18] Foti, F.; Martinelli, L. (2018) A unified analytical model for the self-damping of stranded cables under aeolian vibrations. J. Wind Eng. Ind. Aerodyn. 176, pp. 225–238.

[19] Yu, Y.; Wang, X.; Chen, Z. (2016) A simplified finite element model for structural cable bending mechanism. Int. J. Mech. Sci. 113, pp. 196–210.

[20] Yu, Y.; Chen, Z.; Liu, H.; Wang, X. (2014) Finite element study of behavior and interface force conditions of seven-wire strand under axial and lateral loading. Constr. Build. Mater. 66, pp. 10–18.

[21] Bruski, D. (2020) Determination of the bending properties of wire rope used in cable barrier systems. Materials 13.

[22] Fedorko, G.; Stanova, E.; Molnar, V.; Husakova, N.; Kmet, S. (2014) Computer modelling and finite element analysis of spiral triangular strands. Adv. Eng. Softw. 73, pp. 11–21.

[23] Zhou, B.; Hu, Y.; Zheng, X.; Zhu, H. (2022) Bending behavior of a frictional single-layered spiral strand subjected to multi-axial loads: Numerical and experimental investigation. Appl. Sci. 12.

[24] Poon, C. T.; Barrett, R. A.; Leen, S. B. (2022) Global and local modeling for inter-wire fretting in multi-wire copper conductors. Fatigue Fract. Eng. Mater. Struct. 45, pp. 1618–1634.

[25] Montoya, A.; Waisman, H.; Betti, R. (2012) A simplified contact-friction methodology for modeling wire breaks in parallel wire strands. Comput. Struct. 100–101, pp. 39–53.

[26] Fontanari, V.; Benedetti, M.; Monelli, B. D. (2015) Elasto-plastic behavior of a Warrington-Seale rope: Experimental analysis and finite element modeling. Eng. Struct. 82, pp. 113–120.

[27] Ivanov, H. I.; Ermolaeva, N. S.; Breukels, J.; de Jong, B. C. (2020) Effect of bending on steel wire rope sling breaking load: Modelling and experimental insights. Eng. Fail. Anal. 116, 104742.

[28] Chang, X. et al. (2025) Mechanical property degradation of transmission wire rope caused by different wear evolution. Lubricants 13, 59.

[29] SKF (n.d.) C 6910 V Full complement CARB toroidal roller bearing. Manufacturer product data.

[30] VSL International Ltd. (2013) VSL Post-Tensioning Solutions. Technical brochure.

[31] Du, W.; Ma, B.; Xie, Z.; Cao, D.; Wu, P. (2017) Finite element analysis on the wire breaking rule of 1×7IWS steel wire rope. MATEC Web Conf. 108, 01002.

[32] ANSI/AISC 341-16 (2016) Seismic Provisions for Structural Steel Buildings. American Institute of Steel Construction.

[33] Dassault Systèmes (2024) SOLIDWORKS 2024 [software].

[34] Dassault Systèmes (2024) SIMULIA Abaqus/CAE and Abaqus/Standard, Release 2024 [software].

[35] ANSYS, Inc. (2024) ANSYS Mechanical, Release 2024 R2 (24.2) [software].

[36] EN 1998-1 (2013) Eurocode 8: Design of Structures for Earthquake Resistance – Part 1: General Rules, Seismic Actions and Rules for Buildings.

[37] Le, T.-T.; Asteris, P. G.; Lemonis, M. E. (2022) Prediction of axial load capacity of rectangular concrete-filled steel tube columns using machine learning techniques. Eng. Comput. 38, pp. 3283–3316.

[38] Chliveros, G.; Kontomaris, S. V.; Letsios, A. (2023) Automatic identification of corrosion in marine vessels using decision-tree imaging hierarchies. Eng. 4, pp. 2090–2099.

[39] Rodopoulos, C. A.; Chliveros, G. (2008) Fatigue damage in polycrystals – Part 1: The numbers two and three. Theor. Appl. Fract. Mech. 49, pp. 61–76.

[40] Rodopoulos, C. A.; Chliveros, G. (2008) Fatigue damage in polycrystals – Part 2: Intrinsic scatter of fatigue life. Theor. Appl. Fract. Mech. 49, pp. 77–97.

[41] Ridge, I. M. L.; Zheng, J.; Chaplin, C. R. (2000) Measurement of cyclic bending strains in steel wire rope. J. Strain Anal. Eng. Des. 35, pp. 545–558.

[42] Onur, Y.; İmrak, C.; Onur, T. Ö. (2017) Investigation on bending over sheave fatigue life determination of rotation resistant steel wire rope. Exp. Tech. 41.